

Ca SUBSTITUTION IN LI-POOR ALUMINOUS TOURMALINE

DARRELL J. HENRY

Department of Geology and Geophysics, Louisiana State University, Baton Rouge, Louisiana 70803, U.S.A.

BARBARA L. DUTROW¹

Institut für Mineralogie, Ruhr-Universität, D-4630 Bochum 1, West Germany

ABSTRACT

In a sample of a chemically zoned, low-Li aluminous tourmaline from the amphibolite wallrock of a pegmatite in Maine, the substitutional scheme that appears to exert the dominant control over the incorporation of Ca is $XCa + YMg + O = X\Box + YAl + OH$. A series of hypothetical Ca-incorporation substitution schemes for tourmaline can be established using exchange-vector representations. However, for the zoned Mg-rich tourmaline porphyroblast considered here, most of these alternative schemes can be eliminated. Using exchange-vector diagrams, minor substitution in accordance with the exchange vectors $CaMgNa_{-1}Al_{-1}$ and $AlOMg_{-1}(OH)_{-1}$ was also recognized in this zoned tourmaline. To further test the validity of the substitution $CaMgO\Box_{-1}Al_{-1}(OH)_{-1}$, a tourmaline of composition $CaMg_3Al_6(BO_3)_3Si_6O_{18}O(OH)_3$ was synthesized at 820°C and 20 kbars. The proposed substitution also can account for a large proportion of Ca-incorporation in low-Li aluminous tourmaline from a number of different bulk-compositions if complete analytical data-sets are utilized and the data are projected using exchange vectors to reduce the multicomponent system to the appropriate simplified subsystem.

Keywords: tourmaline, calcium substitution, exchange vectors, crystal chemistry, Maine, amphibolite, experimental synthesis.

SOMMAIRE

Dans un échantillon zoné de tourmaline magnésienne alumineuse à faible teneur en Li, provenant d'un encaissant amphibolitique d'une pegmatite dans le Maine, le schéma de substitution prédominant pour expliquer l'incorporation du Ca serait $XCa + YMg + O = X\Box + YAl + OH$. Nous pouvons écrire une série de schémas différents, représentés par des vecteurs d'échange. Toutefois, pour notre échantillon porphyroblastique, la plupart des alternatives peuvent être éliminées. Dans des diagrammes conçus pour représenter les vecteurs d'échanges, les substitutions $CaMgNa_{-1}Al_{-1}$ et $AlOMg_{-1}(OH)_{-1}$ sont présentes mais jugées mineures. Afin de vérifier la validité de la substitution $CaMgO\Box_{-1}Al_{-1}(OH)_{-1}$, nous avons synthétisé une tourmaline ayant la composition $CaMg_3Al_6(BO_3)_3Si_6O_{18}O(OH)_3$ à 820°C et 20 kbars. Ce schéma de substitution

peut aussi expliquer en grande partie l'incorporation du calcium dans plusieurs compositions différentes de tourmaline alumineuse à faible teneur en Li si les données analytiques complètes sont utilisées et si elles sont interprétées au moyen de projections de vecteurs d'échange, afin de réduire le système à composants multiples à un sous-système simplifié approprié.

(Traduit par la Rédaction)

Mots-clés: tourmaline, incorporation du Ca, vecteurs d'échange, chimie cristalline, Maine, amphibolite, synthèse.

INTRODUCTION

Tourmaline is a common accessory mineral that has been found in virtually all major rock types. It is a useful petrogenetic indicator because it is ubiquitous, chemically and mechanically stable, and has extensive compositional variations that typically reflect the environment in which it crystallized (Henry & Guidotti 1985). However, numerous uncertainties remain regarding the crystal chemistry of tourmaline. One of these regards the mechanism(s) by which Ca is incorporated into the tourmaline structure, which is the subject of this communication.

Tourmaline is a structurally and chemically complex borosilicate mineral that has the general formula $XY_3Z_6(BO_3)_3Si_6O_{18}(OH)_4$. Excellent illustrations of the tourmaline structure can be found in Dietrich (1985), Weiner & Glas (1985) and Gonzales-Carreño *et al.* (1988). However, some of the important structural elements can be summarized as follows. Corner-sharing tetrahedra form hexagonal rings and are principally occupied by Si, although minor ^{IV}Al is found in some cases (Barton 1969, Plyusnina & Voskresenskaya 1974, Foit & Rosenberg 1979, Rosenberg & Foit 1985, Rosenberg *et al.* 1986). Boron is in triangular coordination and has no known substituents (Tsang & Ghose 1973, Povondra 1981). OH groups can occupy two structurally distinct positions: the center of the hexagonal rings, and the corner of brucite-like fragments of three edge-sharing octahedra (Gonzales-Carreño *et al.* 1988). At the central OH site, the principal substi-

¹Present address: Department of Geology and Geophysics, Louisiana State University, Baton Rouge, Louisiana 70803, U.S.A.

TABLE 1. SOME IMPORTANT NATURALLY OCCURRING AND SYNTHETIC TOURMALINE END-MEMBERS

End-member	Formula
Schorl	$\text{NaFe}^{2+}_3\text{Al}_6(\text{BO}_3)_3\text{Si}_6\text{O}_{18}(\text{OH})_4$
Dravite	$\text{NaMg}_3\text{Al}_6(\text{BO}_3)_3\text{Si}_6\text{O}_{18}(\text{OH})_4$
Elbaite	$\text{Na}(\text{Li}_{1.5}\text{Al}_{1.5})\text{Al}_6(\text{BO}_3)_3\text{Si}_6\text{O}_{18}(\text{OH})_4$
Liddicoatite	$\text{Ca}(\text{Li}_2\text{Al})\text{Al}_6(\text{BO}_3)_3\text{Si}_6\text{O}_{18}(\text{OH})_4$
Uvite	$\text{CaMg}_3(\text{MgAl}_5)(\text{BO}_3)_3\text{Si}_6\text{O}_{18}(\text{OH})_4$
Feruvite	$\text{CaFe}_3(\text{MgAl}_5)(\text{BO}_3)_3\text{Si}_6\text{O}_{18}(\text{OH})_4$
Buergerite	$\text{NaFe}^{3+}_3\text{Al}_6(\text{BO}_3)_3\text{Si}_6\text{O}_{18}(\text{O}_3\text{F})$
Chromdravite	$\text{NaMg}_3\text{Cr}_6(\text{BO}_3)_3\text{Si}_6\text{O}_{18}(\text{OH})_4$
Ferridravite	$\text{NaMg}_3\text{Fe}^{3+}_6(\text{BO}_3)_3\text{Si}_6\text{O}_{18}(\text{OH})_4$
Alkali-free tourmaline	$\square(\text{Mg}_2\text{Al})\text{Al}_6(\text{BO}_3)_3\text{Si}_6\text{O}_{18}(\text{OH})_4$

TABLE 2. SELECTED SUBSTITUTION SCHEMES AND CORRESPONDING EXCHANGE-VECTORS KNOWN IN NATURAL TOURMALINE

Site substitutions	Exchange Vectors
$\text{YFe}^{2+} = \text{YMg}^*$	FeMg_{-1}
$\text{YMn} = \text{YMg}$	MnMg_{-1}
$\text{ZFe}^{3+} = \text{ZAl}$	FeAl_{-1}
$\text{ZCr} = \text{ZAl}$	CrAl_{-1}
$\text{ZV} = \text{ZAl}$	VAl_{-1}
$\text{F} = \text{OH}$	FOH_{-1}
$\text{Cl} = \text{OH}$	ClOH_{-1}
$\text{YLi} + \text{YAl} = 2\text{YFe}^+$	LiAlFe_{-2}
$2\text{X}\square^{\#} + \text{YAl} = 2\text{XNa} + \text{YLi}$	$\square_{-2}\text{AlNa}_{-2}\text{Li}_{-1}$
$\text{YAl} + 2\text{O} = \text{YLi} + 2\text{OH}$	$\text{AlO}_2\text{Li}_{-1}(\text{OH})_{-2}$
$\text{X}\square + \text{OH} = \text{YLi} + \text{O}$	$\square\text{OHLi}_{-1}\text{O}_{-1}$
$2\text{XCa} + \text{YLi} = 2\text{XNa} + \text{YAl}$	$\text{Ca}_2\text{LiNa}_{-2}\text{Al}_{-1}$
$\text{XCa} + \text{ZMg} = \text{XNa} + \text{ZAl}$	$\text{CaMgNa}_{-1}\text{Al}_{-1}$
$\text{X}\square + \text{YAl} = \text{XNa} + \text{YMg}$	$\square\text{AlNa}_{-1}\text{Mg}_{-1}$
$\text{YAl} + \text{O} = \text{YMg} + \text{OH}$	$\text{AlOMg}_{-1}(\text{OH})_{-1}$
$\text{YFe}^{3+} + \text{O} = \text{YFe}^{2+} + \text{OH}$	$\text{Fe}^{3+}\text{OFe}^{2+}_{-1}(\text{OH})_{-1}$
$\text{XMg} + \text{YMg} = \text{XNa} + \text{YAl}$	$\text{Mg}_2\text{Na}_{-1}\text{Al}_{-1}$
$\text{YAl} + \text{TAl} = \text{YMg} + \text{TSi}$	$\text{Al}_2\text{Mg}_{-1}\text{Si}_{-1}$
$\text{YTi} + 2\text{TAl} = \text{YMg} + 2\text{TSi}$	$\text{TiAl}_2\text{Mg}_{-1}\text{Si}_{-2}$
$\text{YTi} + \text{YMg} = 2\text{YAl}$	TiMgAl_{-2}

* Superscripts represent site assignments corresponding to the general structural formula.

Represents a vacancy at the X site.

tients include F and Cl (Fuge & Power 1969, Némec 1969, Foit & Rosenberg 1977, Burt 1989). At the OH sites associated with the brucite-like fragments, O^{2-} is the dominant substituent (Foit & Rosenberg 1977, Burt 1989). There are two types of octahedra: the Y octahedra and the slightly smaller, distorted Z octahedra. The Y and Z octahedra share edges to form the brucite-like fragments, and the Z octahedra also share edges with other Z octahedra in a helical linkage parallel to the c axis. The Y octahedra contain diverse cations of different charges (1^+ , 2^+ , 3^+ and 4^+). In most cases, Al predominates in the Z site, but significant amounts of Fe^{2+} , Fe^{3+} , Ti, Mg, Cr and V^{3+} can replace Al.

The nine-coordinated X site commonly contains Na, but may also accommodate Ca, vacancies, and possibly minor amounts of Mg (Donnay & Buerger 1950, Rosenberg & Foit 1979, 1985, Werdinger & Schreyer 1984). Several of the important naturally occurring and synthetic tourmaline end-members are given in Table 1.

Within this spectrum of possible substituents, potential chemical variations in tourmaline may be represented by an array of homovalent or heterovalent substitutional schemes (Table 2) that also can be written in terms of compositional exchange-vectors (cf. Thompson 1982, Burt 1988, 1989). However, because many different combinations of exchange vectors can equally well describe the actual composition of a tourmaline, other criteria must be used to give the most significant schemes of substitution in terms of its crystal chemistry. One such criterion is developed through the investigation of compositional variations in chemically zoned grains. Because initial, intermediate, and final compositions are known, the exchange vector that relates them can be determined directly (Hewitt & Abrecht 1986). Because the extent of zoning in minerals is typically limited, further verification of a particular substitution scheme can be obtained if a composition(s) along the exchange vector (or its extension) can be experimentally synthesized (cf. Abrecht & Hewitt 1988).

Although Ca is an important substituent for Na in tourmaline, the mechanism of its incorporation has not been examined in detail (cf. Foit & Rosenberg 1977). Coupled substitutions must be involved. The two most common of these are the $\text{CaMgNa}_{-1}\text{Al}_{-1}$ and $\text{Ca}_2\text{LiNa}_{-2}\text{Al}_{-1}$ exchange vectors that, starting from *dravite*, lead to the uvite and liddicoatite end-members, respectively (Table 1). These schemes are most extensively developed in tourmaline from low-Al metacarbonate rocks and Li-rich pegmatites, respectively (Henry & Guidotti 1985). In other tourmaline-bearing rock types, Al contents are normally higher and Li contents are lower (e.g., Foit & Rosenberg 1977). Tourmaline in such rocks contains enough Al to fill the Z site, and substantial amounts of Al are located at the Y site as a consequence of the substitutions $\text{AlOMg}_{-1}(\text{OH})_{-1}$, $\square\text{AlNa}_{-1}\text{Mg}_{-1}$, or both (Table 2). Nonetheless, aluminous tourmaline can contain a substantial amount of Ca (Henry & Guidotti 1985). Consequently, there is probably an additional mechanism(s) that permits incorporation of Ca in natural Li-poor aluminous tourmaline.

Possible schemes for incorporation of Ca in aluminous tourmaline can be visualized graphically using a prism defined by the additive component *dravite* [an arbitrary fixed starting point in composition space (cf. Thompson 1982)] and the $\text{CaMgNa}_{-1}\text{Al}_{-1}$, $\text{AlOMg}_{-1}(\text{OH})_{-1}$ and $\square\text{AlNa}_{-1}\text{Mg}_{-1}$ exchange

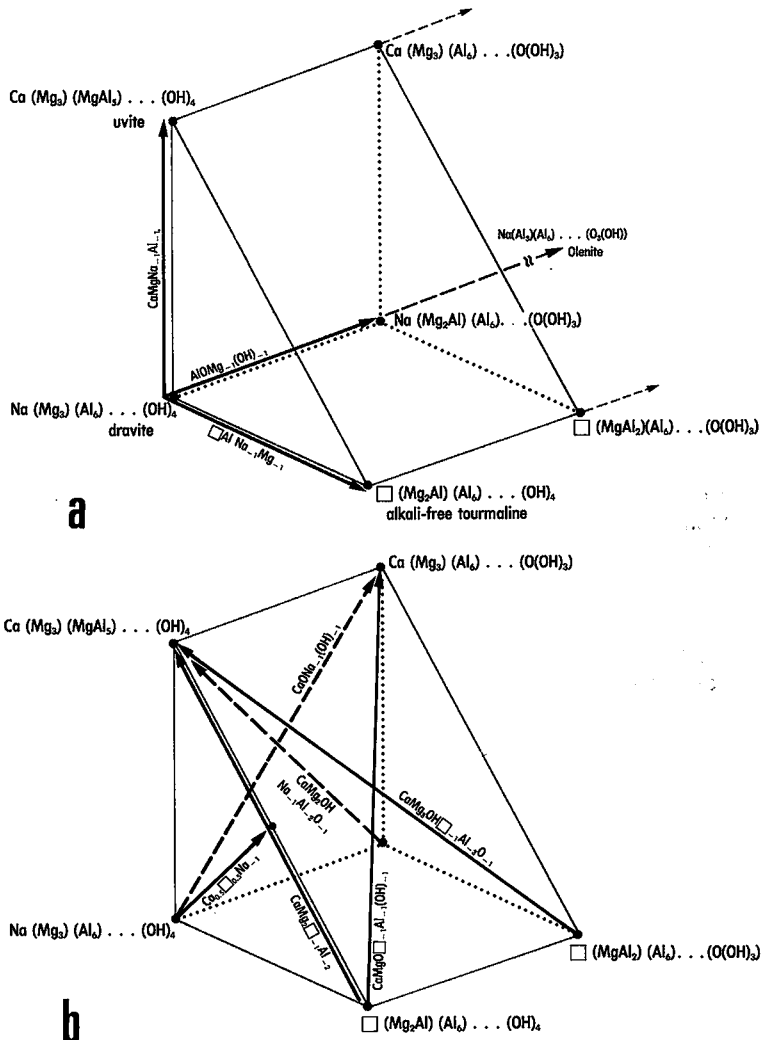


FIG. 1. Compositional prism for Li-poor aluminous tourmaline. (a) Compositional prism generated by a single application of the three exchange-vectors ($\text{CaMgNa}_{-1}\text{Al}_{-1}$, $\text{AlOMg}_{-1}(\text{OH})_{-1}$ and $\square\text{AlNa}_{-1}\text{Mg}_{-1}$) to the dravite additive component. This representation defines the typical range of composition space that can introduce Ca and additional Al into tourmaline. The vectors are shown as bold arrows. The intermediate parts of the tourmaline formulae are given as dots because they are not affected by the exchange operation, but are understood to be present. Operation of the exchange vector $\text{AlOMg}_{-1}(\text{OH})_{-1}$ three times on the dravite additive component produces the olenite end-member. (b) Possible additional exchange-vectors (bold arrows; dashed on the back face) that can introduce Ca into tourmaline.

vectors (Fig. 1a). This type of diagram is particularly useful because data from structural formulae can be directly plotted without renormalization (and the possible masking of important information), as in the more conventional X - Y orthogonal plots or barycentric triangle plots (Burt 1989). Although dravite is used as the additive component, the compo-

sitions in natural multicomponent tourmaline can be "projected" down other exchange vectors to the assumed simplified system simply by adding or subtracting the appropriate amount of cation(s) involved in the exchange operation. For example, Fe^{2+} -bearing tourmaline can be projected into the Mg-subsystem by adding all the Fe^{2+} to Mg in

TABLE 3. POSSIBLE SCHEMES OF SUBSTITUTION FOR THE INCORPORATION OF Ca INTO TOURMALINE

Site substitutions	Exchange Vectors
$XCa + ZMg = XNa + ZAl$	$CaMgNa_{-1}Al_{-1}$
$XCa + YMg = XNa + YAl$	$CaMgNa_{-1}Al_{-1}$
$XCa + O = XNa + OH$	$CaONa_{-1}(OH)_{-1}$
$XCa + YMg + ZMg + OH = XNa + YAl + ZAl + O$	$CaMg_2OHNa_{-1}Al_{-2}O_{-1}$
$0.5XCa + 0.5X\Box = XNa$	$Ca_{0.5}\Box_{0.5}Na_{-1}$
$XCa + YMg + ZMg = X\Box + YAl + ZAl$	$CaMg_2\Box_{-1}Al_{-2}$
$XCa + 2YMg = X\Box + 2YAl$	$CaMg_2\Box_{-1}Al_{-2}$
$XCa + YMg + O = X\Box + YAl + OH$	$CaMgO\Box_{-1}Al_{-1}(OH)_{-1}$
$XCa + 2YMg + ZMg + OH = X\Box + 2YAl + ZAl + O$	$CaMg_3OH\Box_{-1}Al_{-3}O_{-1}$

accordance with the $FeMg_{-1}$ exchange vector. Thus in a multicomponent tourmaline, divalent cations can be treated as Mg (or, more clearly, as Mg^*), and trivalent cations can be treated as Al (or Al^*) (cf. Burt 1989).

In addition to the exchange vector $CaMgNa_{-1}Al_{-1}$, several other Ca exchange vectors are possible. These can be represented by various linear combinations of the $CaMgNa_{-1}Al_{-1}$, $AlOMg_{-1}(OH)_{-1}$, and $\Box AlNa_{-1}Mg_{-1}$ vectors that define the prism (Fig. 1b, Table 3). However, the vector representations provide only a simple graphical depiction of charge restrictions, without reference to stability under particular conditions of crystallization or crystal-chemical constraints. Possible exchange-vectors in terms of crystal chemistry can be assessed using data from zoned Ca-bearing tourmaline crystals in a prism of this type.

In our study of Ca-substitution in tourmaline, two complementary approaches were taken. First, the patterns of compositional zoning in a Ca-rich aluminous tourmaline crystal were examined to constrain possible substitutional schemes. Second, using the substitutional scheme suggested by the zoning, synthesis of the hypothetical end-member phase was attempted.

ZONING IN Ca-RICH ALUMINOUS TOURMALINE

Geological setting and petrography

Potential Ca-substitution schemes in aluminous tourmaline were initially evaluated using material from a tourmaline-rich magnesian amphibolite from the Newry pegmatite mines area, Rumford Quadrangle, northwestern Maine, U.S.A. The magnesian amphibolite, forming part of the wallrock of the gem-bearing pegmatites, contains large (2–5 cm) black tourmaline crystals (30%), amphibole (50%), chlorite (17%), calcite (2%), biotite (1%), pyrite (tr),

apatite (tr) and rutile (tr). The unusual local chemistry and mineralogy of the amphibolite reflect the intense alteration of the wallrock, probably in response to contact metamorphism and accompanying metasomatism (Bastin 1911, Fraser 1930). The polymetamorphic history of northwestern Maine consists of at least three episodes of Devonian regional metamorphism and several deformational events (Guidotti 1970, Holdaway *et al.* 1982, 1988). The pegmatites in this area are suggested to have developed late in the last major metamorphic event (Guidotti, pers. comm.).

The sample shows evidence of an earlier higher-grade assemblage of tourmaline + magnesiohornblende + chlorite(?) + biotite(?) and a subsequent, lower-grade assemblage of tourmaline + actinolitic hornblende + chlorite + biotite + calcite. The amphibole has irregular zoning, with patchy, relict magnesiohornblende generally surrounded by actinolitic hornblende.

The tourmaline grains (>4 mm in cross section) are euhedral (Fig. 2a). The bulk of these post-kinematic porphyroblasts probably developed very late in the metamorphic history, because they incorporate the mineral assemblage of the previously deformed matrix, *i.e.*, zoned magnesiohornblende to actinolitic hornblende, biotite and chlorite. In addition, most of the tourmaline porphyroblasts contain internal regions (5–30% of the total area) that have a weak blue pleochroism, feathery lamellar features, and generally no mineral inclusions. These internal zones, designated Zone 1, contain heterogeneous lamellar features that probably represent an early generation of rapidly crystallizing tourmaline (Fig. 2b). The outer zones, designated Zone 2, have a weak pale green pleochroism, fewer, less well-developed lamellar features, and inclusions of matrix minerals (Fig. 2a).

Mineral chemistry and tourmaline zoning

Minerals were imaged with back-scattered electrons (BSE) and quantitatively analyzed by wavelength-dispersion spectrometry (WDS) using the automated JEOL 733 electron microprobe at Louisiana State University. Digital BSE images were obtained with an accelerating potential of 15 kV and 10 nA and processed with the Tracor Northern 5700 image-analysis system. WDS analyses were done at 15 kV accelerating potential and 20 nA sample current. The electron beam was focused to a 1- μ m spot for the microprobe traverse of the zoned tourmaline, and was defocused to a 5- μ m spot for the analyses of associated minerals. Well-characterized synthetic and natural silicates and carbonates were used as standards, and the data were corrected on line with the procedure of Bence & Albee (1968). The analytical uncertainty for each element was determined

from replicate analyses of selected standards (Fig. 3). To assess the effects of different schemes of normalization, the tourmaline compositions were normalized on the basis of both 29 atoms of oxygen (assuming three B cations) and 15 cations (exclusive of Na, Ca and K). The amount of B_2O_3 necessary to produce three B cations in the structural formula was calculated from stoichiometric constraints. The bases of normalization of the other minerals analyzed are given in Table 4.

Compositional variations in minerals associated with the tourmaline reflect the polymetamorphic nature of the sample (Table 4). The amphibole grains that are found in the matrix and as inclusions in tourmaline are chemically heterogeneous in an irregular fashion, and range from magnesiohornblende to actinolite, with $Mg/(Mg + Fe)_T$ from 0.77 to 0.87. In general, the amphibole becomes more actinolitic during the later stages of development, such that it becomes depleted with respect to Tschermaks ($Al_2Mg_{-1}Si_{-1}$) and glaucophane components ($NaSiCa_{-1}Al_{-1}$), as well as $FeMg_{-1}$. The biotite is phlogopitic, with minor amounts of Ti and F, and an $Mg/(Mg + Fe)_T$ of 0.79. The chlorite has minor chemical variability, with Al ranging from 5.08 to 5.25 (based on 28 oxygen atoms) and $Mg/(Mg + Fe)_T$ from 0.81 to 0.82. Calcite is nearly pure $CaCO_3$, with $Mg/(Ca + Mg + Fe)_T = 0.0087$ and $Fe_T/(Ca + Mg + Fe)_T = 0.0029$.

The tourmaline chemistry also reflects the bulk composition of the rock (Table 5). The chemically zoned tourmaline is close to the dravite end-member, with $Mg/(Mg + Fe)_T$ ranging from 0.86 to 0.88, Na, 0.51 to 0.58 apfu (atoms per formula unit), Mg, 2.21 to 2.47 apfu, Fe_T , 0.33 to 0.36 apfu, and Al_T , 6.05 to 6.29 apfu. However, there are significant and variable amounts of Ca (0.19–0.36 cations) and X-site vacancies (0.09–0.23); therefore, exchange vectors that account for Ca- and X-site vacancies also must be important in this tourmaline. In addition, there are only minor amounts of Ti, Cr, Mn, Ni, K and F, and the Fe_T contents are essentially constant. Furthermore, Li contents are thought to be insignificant because tourmaline that contains significant amounts of Mg typically have very minor Li contents (Foit & Rosenberg 1977, Wilson & Long 1983, Grew & Sandiford 1984). Consequently, this zoned tourmaline is an ideal sample for a detailed investigation of Ca-incorporation in the simplified Mg-bearing subsystem, as there are limited additional competing substitutions.

A detailed compositional traverse of a representative tourmaline porphyroblast (Fig. 3) shows that the tourmaline is progressively enriched in Ca and Mg and depleted in Al, Na and X-site vacancies from the core (Zone 1) to the rim. Despite having heterogeneous lamellar features in BSE images (Fig. 2b), Zone 1 has only a small amount of compositional

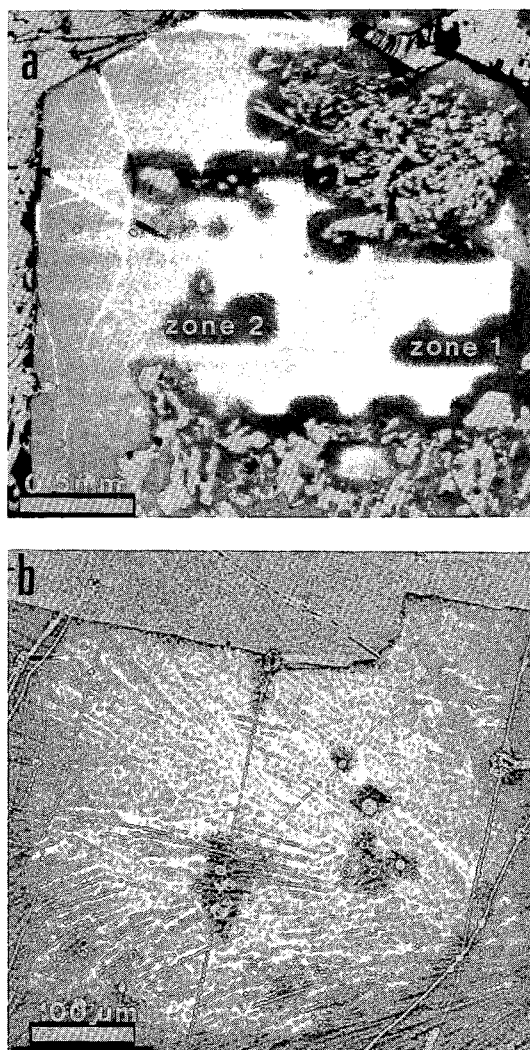


FIG. 2. Back-scattered electron images of a tourmaline porphyroblast from the magnesian amphibolite from Maine. (a) Euhedral tourmaline porphyroblast (shades of medium grey) with grains of amphibole, chlorite and biotite (white) in the matrix and as inclusions in the tourmaline. Zones 1 and 2 and the path of the detailed quantitative analyses are shown. (b) Digital image-processed interface between the interior Zone 1 and Zone 2 parts of the tourmaline. Note the feathery intergrowth features suggestive of rapid crystallization.

variability: slight decreases are found in Al and Mg from the innermost core to the Zone 1 - Zone 2 interface. No obvious compositional discontinuities are observed on a small scale in this feathery lamellar region (Zone 1), probably owing to excitation volumes under the electron beam that are larger than the lamellar features ($< 5 \mu m$) and the $50\text{-}\mu m$ ana-

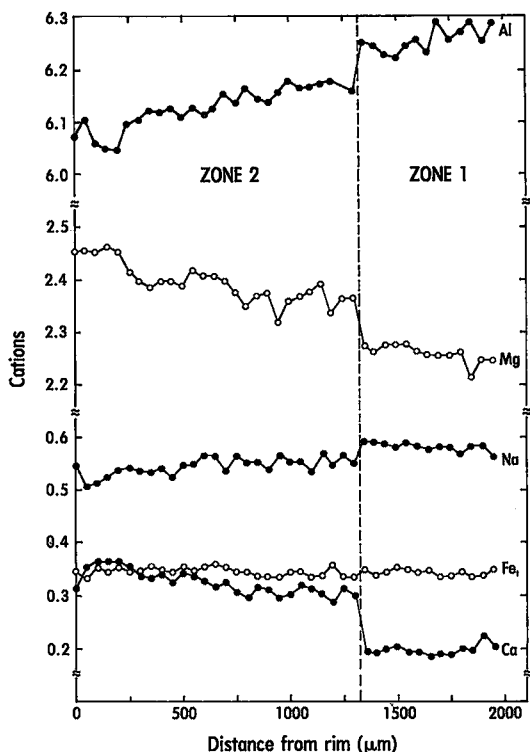


FIG. 3. Compositional zoning of a representative tourmaline porphyroblast from the magnesian amphibolite. The tourmaline porphyroblast was analyzed at 50- μm intervals along the path shown in Figure 2a. Based on replicate analyses of selected standards, the analytical uncertainties (in cation units) are 0.015 for Mg, 0.010 for X-site vacancies, 0.008 for Na, 0.005 for Al and Fe, and 0.002 for Ca.

lytical step interval. At the Zone 1 - Zone 2 interface, there is a sharp compositional discontinuity in Al, Mg, Ca and (to a lesser extent) Na. The outer part of the tourmaline (Zone 2) has continuous and significant zoning from the Zone 1 - Zone 2 interface to the rim. The overall pattern of zonation presumably reflects a late-stage tourmaline-forming reaction that locally involves incomplete depletion of the Tschermaks and glaucophane components from the magnesiohornblende in the matrix to form more actinolitic zones in the amphibole. The entire set of tourmaline compositional data used in this traverse have been submitted to the Depository of Unpublished Data, CISTI, National Research Council of Canada, Ottawa, Canada K1A 0S2.

Because of the extent of Ca-zoning within the porphyroblast, it is possible to isolate the dominant substitutional mechanism(s) using the compositional prism (Figs. 1a, b). However, it is difficult to effec-

tively represent the array of data points within this three-dimensional prism. Consequently, a series of projections of both the tourmaline data and the exchange vectors were made onto the side face (Fig. 4a), back face (Fig. 4b) and basal face (Fig. 4c) of the prism. These three diagrams are somewhat unorthodox in that they do not involve renormalization of a set of plotting parameters but allow mineral formulae to be plotted directly (*cf.* Burt 1988, 1989). Because Fe_i is constant and the other divalent constituents are minor, Mg is plotted directly without projecting the composition to the Mg subsystem.

The side projection (Fig. 4a) is restricted to the X-site substituents: X-site vacancies, Ca and Na (Na could also be plotted on this diagram as a series of isopleths parallel to the diagonal). The tourmaline data fall into two groups: Zone-1 and Zone-2 tourmalines (data normalized to 29 oxygen atoms). However, the data fall on a curvilinear trend that is roughly parallel to the diagonal and the exchange vectors: $\text{CaMgO}\square_{-1}\text{Al}_{-1}(\text{OH})_{-1}$, $\text{CaMg}_2\square_{-1}\text{Al}_{-2}$ and $\text{CaMg}_3\text{OH}\square_{-1}\text{Al}_{-3}\text{O}_{-1}$. In the more Ca-rich compositions, the slight dispersion of the data toward the Ca apex (in excess of the analytical uncertainty) suggests that with an increase in Ca, the tourmaline may be influenced, to a lesser degree, by one or more of the exchange vectors: $\text{CaMgNa}_{-1}\text{Al}_{-1}$, $\text{CaONa}_{-1}(\text{OH})_{-1}$ and $\text{CaMg}_2\text{OHNa}_{-1}\text{Al}_{-2}\text{O}_{-1}$. However, the predominant Ca-substitution must be one of those defined by the diagonal exchange-vectors.

The back-face (Fig. 4b) and basal-face projections (Fig. 4c) involve cations at more than one structural site. Because the proportion of OH was not determined, other parameters must be used to locate the data points on these diagrams. Projected isopleths of Al (Al' and Al'' in Figs. 4b and 4c, respectively) are used for this purpose (projected isopleths of Mg also could have been used). The data again fall into the Zone-1 and Zone-2 groups. In both diagrams, the data show a trend that is roughly parallel to the projected Al isopleths. This parallelism is consistent with the exchange vectors $\text{CaONa}_{-1}(\text{OH})_{-1}$ and $\text{CaMgO}\square_{-1}\text{Al}_{-1}(\text{OH})_{-1}$ in Figure 4b and with the exchange vector $\text{CaMgO}\square_{-1}\text{Al}_{-1}(\text{OH})_{-1}$ in Figure 4c. However, both of these plots show a horizontal dispersion of the Zone-1 data (well beyond analytical uncertainty). The exchange vectors that are common to the minor horizontal dispersion of data in both of these plots are FeAl_{-1} and $\text{AlOMg}_{-1}(\text{OH})_{-1}$. Because Fe_i is constant and Al and Mg are inversely related in Zone 1, the exchange vector that accounts for this minor trend of data is $\text{AlOMg}_{-1}(\text{OH})_{-1}$. The locally variable $\text{AlOMg}_{-1}(\text{OH})_{-1}$ component is presumably reflected by the lamellar features that are most prominently developed in Zone 1. In the more Ca-rich compositions, there is some vertical scatter of the data. Compared to the dispersion of data from the Ca-rich compositions in Figure 4a, this

TABLE 4. REPRESENTATIVE MINERAL COMPOSITIONS OF ASSOCIATED MINERALS IN THE AMPHIBOLITE

AMPHIBOLE					BIOTITE			CHLORITE		
Analysis pt. Remarks	1 matrix rim	2 matrix core	7 inclusion	13 inclusion	Analysis pt. Remark	13 matrix	1 inclusion	Analysis pt. Remark	6 matrix	14 inclusion
SiO ₂ (wt %)	54.19	48.13	51.98	45.61	SiO ₂	40.01	40.08	SiO ₂	28.54	28.13
Al ₂ O ₃	3.96	11.22	7.28	13.78	Al ₂ O ₃	17.68	18.17	Al ₂ O ₃	22.06	22.50
TiO ₂	0.06	0.13	0.17	0.32	Cr ₂ O ₃	0.00	0.10	Cr ₂ O ₃	0.03	0.19
Cr ₂ O ₃	0.00	0.01	0.03	0.04	TiO ₂	0.52	0.37	TiO ₂	0.02	0.02
FeO*	5.53	6.88	5.83	7.30	FeO	8.09	8.00	FeO	10.22	9.78
MgO	19.92	16.42	18.08	14.74	MnO	0.08	0.11	MnO	0.12	0.09
MnO	0.13	0.19	0.15	0.12	MgO	17.22	17.36	MgO	25.18	24.77
NiO	0.04	0.03	0.03	0.01	NiO	0.00	0.00			
CaO	12.75	12.27	12.54	12.24	CaO	0.03	0.06			
Na ₂ O	0.57	1.78	1.19	2.12	Na ₂ O	0.06	0.06			
K ₂ O	0.07	0.14	0.08	0.20	K ₂ O	9.67	9.61			
F	0.10	0.08	0.06	0.06	BaO	0.03	0.00			
					F	0.22	0.21			
Total	97.31	97.38	97.41	96.54	Total	93.61	94.12			
O=F	0.04	0.03	0.03	0.03	O = F	0.09	0.09			
TOTAL	97.27	97.24	97.39	96.51	TOTAL	93.52	94.03			
Atomic proportions on the basis of 23 oxygen atoms					22 oxygen atoms			28 oxygen atoms		
Si	7.585	6.842	7.298	6.569	Si	5.823	5.793	Si	5.613	5.566
Al	0.415	1.158	0.702	1.431	Al	2.177	2.207	Al	2.387	2.434
Al	0.238	0.721	0.503	0.909	Al	0.855	0.890	Al	2.728	2.814
Ti	0.006	0.014	0.018	0.034	Cr	0.000	0.012	Cr	0.005	0.030
Cr	0.000	0.002	0.003	0.005	Ti	0.057	0.040	Ti	0.003	0.004
Fe	0.597	0.781	0.684	0.879	Fe	0.965	0.967	Fe	1.682	1.618
Mg	4.154	3.478	3.784	3.164	Mn	0.010	0.013	Mn	0.019	0.016
Mn	0.000	0.000	0.005	0.008	Mg	3.734	3.740	Mg	7.379	7.305
Ni	0.005	0.004	0.003	0.001	Ni	0.000	0.000	Ni	0.008	0.005
C Total	5.000	5.000	5.000	5.000	Total	5.641	5.662	Total	11.824	11.792
Fe	0.050	0.037	0.000	0.000	Ca	0.004	0.009			
Mn	0.015	0.023	0.013	0.006	Na	0.016	0.016			
Ca	1.912	1.868	1.886	1.889	K	1.796	1.772			
Na	0.023	0.072	0.114	0.105	Ba	0.002	0.000			
B Total	2.000	2.000	2.000	2.000	Total	1.817	1.796			
Na	0.132	0.420	0.210	0.486	F	0.102	0.095			
K	0.013	0.025	0.014	0.036						
A Total	0.145	0.445	0.224	0.522						
F	0.040	0.036	0.028	0.028						

*all Fe assumed to be FeO

scatter in the more Ca-rich compositions is consistent with the exchange vector $\text{CaMgNa}_{-1}\text{Al}_{-1}$. Thus the overall dispersion in the Zone-2 data is probably the result of a combination of $\text{AlOMg}_{-1}(\text{OH})_{-1}$ and $\text{CaMgNa}_{-1}\text{Al}_{-1}$ components.

The exchange component that is responsible for the general trend of the array of data on all three projections is the vector: $\text{CaMgO}\square_{-1}\text{Al}_{-1}(\text{OH})_{-1}$. If the tourmaline data also are normalized to a 15-cation basis (exclusive of Na, Ca and K), there is a minor shift in the absolute position of the data points, but the relative trend is retained in all plots. Interestingly, if the data are projected to a Ca-free basis (Figs. 4a, c), these tourmaline compositions would have maximum X-site vacancies of 0.4–0.5 and OH of 3.9–4.0. This projected Ca-free starting point represents a tourmaline composition that could have developed in a Ca-free environment, and as a result of the exchange vector $\square\text{AlNa}_{-1}\text{Mg}_{-1}$. This alkali-deficient composition, in turn, reflects the moderately aluminous and Na-poor nature of the rock.

SYNTHESIS OF Ca-Mg DEPROTONATED TOURMALINE

Supporting evidence for the substitution mechanism $\text{CaMgO}\square_{-1}\text{Al}_{-1}(\text{OH})_{-1}$ was sought in high-pressure, high-temperature experiments. Because an alkali-free tourmaline with the composition $\square(\text{Mg}_2\text{Al})\text{Al}_6(\text{BO}_3)_3\text{Si}_6\text{O}_{18}(\text{OH})_4$ had been successfully synthesized at 870°C and 20 kbars (Werdning & Schreyer 1984), this composition was used as the arbitrary starting point for the $\text{CaMgO}\square_{-1}\text{Al}_{-1}(\text{OH})_{-1}$ exchange operation (as in Fig. 1b). This hypothetical exchange-operation leads to the composition $\text{CaMg}_3\text{Al}_6(\text{BO}_3)_3\text{Si}_6\text{O}_{18}\text{O}(\text{OH})_3$. Synthesis of this composition was attempted under conditions similar to those used by Werdning & Schreyer (1984).

Starting materials consisted of constituent oxides (CaCO_3 , MgO , $\tau\text{-Al}_2\text{O}_3$, SiO_2) combined in the stoichiometric proportions of the hypothetical tourmaline. In accordance with the procedure of Werdning & Schreyer (1984), B and water were added in excess amounts. A known amount of crystalline H_3BO_3 (No. 165 Merck; 100% excess to insure B

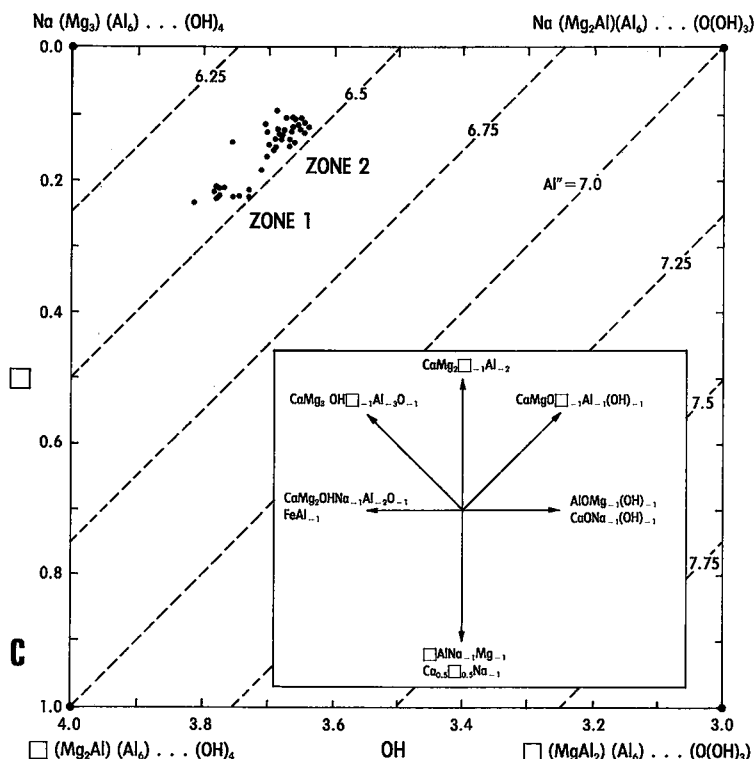


FIG. 4. Projections onto various faces of the tourmaline compositional prism. (a) Side-face projection with possible exchange-vectors (see inset). (The arrows labeled with the exchange vectors represents the direction of the vector but not necessarily the length of the vector in this and subsequent figures.) (b) Back-face projection; the data are plotted using Ca and the projected Al isopleths (Al') using the formula: $Al' = Al_t - X\text{-site vacancies}$. (c) Basal-face projection; the data are plotted using X-site vacancies and the projected Al isopleths (Al'') using the formula: $Al'' = Al_t + Ca$. The analytical uncertainties for data plotted on these diagrams are 0.015 for Al', 0.010 for X-site vacancies and 0.008 for Al''.

saturation) was added because buffering of B_2O_3 fugacity is not currently possible. The above materials were thoroughly mixed by grinding under acetone. Because hydronium (H_3O^+) substitution at the X site is unlikely in tourmaline (Werdinger & Schreyer 1984), excess H_2O was added to this mixture. The oxide mixture was placed in a welded gold capsule, distilled water was added, the capsule was sealed and tested for leaks, and run in a piston-cylinder apparatus at $820^\circ C$ and 20 kbars for 72 hours. The piston-cylinder techniques used here are essentially those given by Massonne & Schreyer (1986).

Upon completion of the synthesis experiment, excess boric acid was largely removed by washing in warm water, and the products were mounted for imaging and analysis using scanning electron microscopy (SEM), energy-dispersion spectrometry

(EDS) and X-ray diffraction (XRD). Observations with the SEM showed tourmaline to be the only phase present (other than the excess boric acid that remained after washing) in the products.

Tourmaline formed well-developed, euhedral, nearly equant grains that range in size from 5 to 25 μm (Fig. 5). The equant morphology is similar to that commonly developed in other Mg-tourmaline species such as dravite, uvite or ferridravite, with trigonal prisms and pyramids forming the prominent faces (*cf.* Dietrich 1985). Minor clusters of elongate tourmaline ($5 \times 0.25 \mu m$ prisms) also formed at the positive end of the c axis (recognized by the steeper pyramidal faces) of the coarser tourmaline crystals (Fig. 5). Interestingly, this is the same end that develops authigenic tourmaline overgrowths on tourmaline detritus (*cf.* Alty 1933). EDS analyses of the large and small tourmaline crystals gave identical

TABLE 5. REPRESENTATIVE COMPOSITIONS ALONG A TRAVERSE THROUGH A ZONED TOURMALINE CRYSTAL

Analysis pt.	1	15	27	28	40
Distance from rim (μm)	0	700	1300	1300	1950
B ₂ O ₃	10.77	10.83	10.80	10.81	10.87
SiO ₂	36.94	36.98	37.12	37.26	37.33
Al ₂ O ₃	31.92	32.53	32.43	32.99	33.35
TiO ₂	0.28	0.25	0.16	0.10	0.13
Cr ₂ O ₃	0.06	0.04	0.01	0.03	0.06
FeO	2.56	2.62	2.49	2.60	2.61
MnO	0.03	0.01	0.01	0.01	0.00
MgO	10.19	10.01	9.86	9.48	9.42
NiO	0.04	0.02	0.00	0.01	0.01
K ₂ O	0.01	0.01	0.00	0.01	0.01
CaO	1.80	1.87	1.74	1.11	1.20
Na ₂ O	1.75	1.72	1.76	1.90	1.83
F	0.10	0.05	0.00	0.00	0.00
Total	96.44	96.94	96.38	96.30	96.81
O=F	0.04	0.02	0.00	0.00	0.00
TOTAL	96.40	96.91	96.38	96.30	96.81
Atomic Proportions on the basis of 29 Oxygen Atoms					
B	3.000	3.000	3.000	3.000	3.000
Si	5.961	5.933	5.976	5.991	5.971
^v Al	0.039	0.067	0.024	0.009	0.029
^z Al	6.000	6.000	6.000	6.000	6.000
^v Al	0.033	0.085	0.130	0.242	0.258
Ti	0.034	0.030	0.019	0.012	0.015
Cr	0.008	0.005	0.001	0.004	0.007
Fe	0.346	0.351	0.335	0.350	0.349
Mn	0.003	0.002	0.001	0.001	0.000
Mg	2.452	2.393	2.366	2.272	2.246
Ni	0.005	0.002	0.000	0.001	0.001
^v Total	2.880	2.868	2.852	2.881	2.876
K	0.001	0.002	0.001	0.001	0.002
Ca	0.310	0.322	0.301	0.192	0.205
Na	0.549	0.536	0.550	0.592	0.568
^x Total	0.860	0.860	0.852	0.785	0.775
F	0.048	0.026	0.000	0.000	0.000

* Calculated on the basis of 3 B atoms per formula unit

compositions. The small prisms probably developed during quenching of the experiment. Unfortunately, the <10 mg yield was insufficient for both SEM-EDS and unit-cell determination (although one was attempted). Nonetheless, the synthesis of single-phase tourmaline with the hypothetical Ca-Mg composition lends further credence to a CaMgO□₋₁Al₋₁(OH)₋₁ deprotonated exchange as a viable Ca-substitution mechanism in aluminous tourmaline.

DISCUSSION

In the strictest sense, the preceding sections have demonstrated that CaMgO□₋₁Al₋₁(OH)₋₁ is the prevailing Ca substitution that can account for the zoning patterns found in the tourmaline from this amphibolite locality. Furthermore, additional evidence for the credibility of this exchange vector as a crystal-chemically viable scheme of substitution was

gained through the synthesis of a hypothetical Ca-Mg deprotonated end-member. However, to be generally important as a substitution scheme, it must be able to account for the observed chemical variations associated with Ca substitution in tourmaline from other settings.

If CaMgO□₋₁Al₋₁(OH)₋₁ is the dominant mechanism of Ca-incorporation in aluminous tourmaline, it should have several predictable consequences. (1) There should be a general inverse correlation between Ca and X-site vacancies, and a poor correlation between Ca and Na in tourmaline from variable host-rock compositions. (2) If complete tourmaline compositional data are available and they are projected into the simplified subsystem using the appropriate exchange-vectors, the data should plot in accordance with the CaMgO□₋₁Al₋₁(OH)₋₁ scheme. (3) This substitution will develop only in tourmaline from rocks with relatively aluminous bulk-compositions, and where X-site vacancies have developed (or can be potentially developed) via □AlNa₋₁Mg₋₁.

A test of the correlation of Ca with other constituents or combinations of constituents in tourmaline from a number of different bulk-compositions was made using the data of Povondra (1981). The tourmaline compositions were evaluated from a variety of igneous rocks, pegmatites, greisens, quartz veins and several metamorphic rock-types, and are primarily from the dravite-schorl series (generally with low Li contents). Povondra (1981) completely analyzed the tourmaline fraction for all major and minor constituents using a combination of gravimetric and spectroscopic methods. The data should thus be internally consistent. In accordance with the presumed aluminous nature necessary for CaMgO□₋₁Al₋₁(OH)₋₁, only the 75 tourmaline compositions containing more than 6 Al apfu (initially assumed to fill the Z site) were used.

For these data, a plot of Ca versus Na shows little or no apparent correlation (Fig. 6a). However, in agreement with the CaMgO□₋₁Al₋₁(OH)₋₁ scheme (and two other Ca exchange vectors), a plot of Ca versus X-site vacancies has a general inverse correlation, such that low-Ca tourmaline (<0.1 cations) typically has an X-site vacancy between 0.25 and 0.5, whereas tourmaline richer in Ca (>0.1 cations) tends to have a significantly lower X-site vacancy (Fig. 6b). Nonetheless, this latter inverse correlation is not very striking, and illustrates one of the potential pitfalls in attempting to discern substitution schemes using rocks with disparate bulk-compositions: the trends will be obscured (dispersed in a vertical direction in Figs. 6a, b) by variable amounts of substitutions such as □AlNa₋₁Mg₋₁ or AlOMg₋₁(OH)₋₁ (or both) that may be found to varying degrees in tourmaline from different bulk-rock compositions. These problems will also be

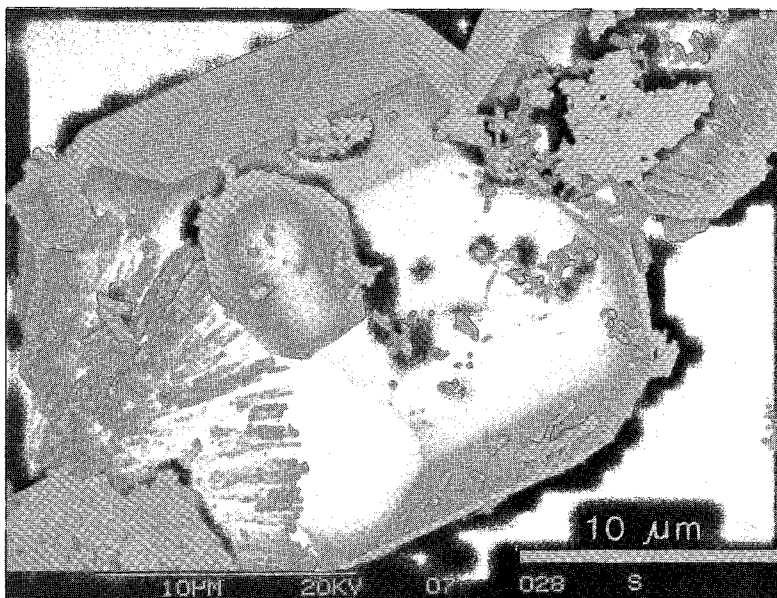


FIG. 5. SEM image of synthetic Ca-Mg deprotonated tourmaline. The smaller crystals are apparently tourmaline grains that nucleated during quenching of the experiment.

present, and perhaps worse, when combining tourmaline data from different bulk-compositions on vector diagrams such as Figure 4.

One way to circumvent the problem of variable bulk-compositions is to reduce complete tourmaline compositions to the Mg-Al subsystem using the appropriate exchange-vectors, and to plot the resulting parameters of the product and reactant of the exchange vector on a standard orthogonal binary diagram. This was done for the $\text{CaMg}^*\text{Na}_{-1}\text{Al}_{-1}$ and $\text{CaMg}^*\text{O}_{-1}\text{Al}_{-1}(\text{OH})_{-1}$ exchange-vectors using the completely characterized data-sets of Povondra. In these diagrams, we assumed that $\text{Mg}^* = \text{Mg} + \text{Fe}^{2+} + \text{Mn} + 2*\text{Li} - \text{Ti}$, $\text{Al}^* = \text{Al} + \text{Fe}^{3+} + 2*\text{Ti} - \text{Li}$, $\text{Na}^* = \text{Na} + \text{K}$ and $\text{OH}^* = \text{OH} + \text{F}$; Ti and Li are minor constituents that are assumed to act in accordance with the exchange vectors TiMgAl_{-2} and LiAlFe_{-2} , respectively (e.g., Henry & Guidotti 1985, Burt 1989).

On plots of $\text{Ca} + \text{Mg}^*$ versus $\text{Na} + \text{Al}^*$ (Fig. 7a) and $\text{Ca} + \text{Mg}^* + \text{O}$ versus $\square + \text{Al}^* + \text{OH}^*$ (Fig. 7b), the Povondra data-set falls approximately along linear arrays. A linear least-squares fit of these data gives a slope of -0.662 ($r=0.81$) for Figure 7a and a slope of -0.833 ($r=0.76$) for Figure 7b. If this Ca substitution scheme [$\text{CaMgO}_{-1}\text{Al}_{-1}(\text{OH})_{-1}$] were to completely account for all of the variations, the data should fall along a line with a slope of -0.5 on the $\text{Ca} + \text{Mg}^*$ versus $\text{Na} + \text{Al}^*$ diagram and with a slope of -1.0 for $\text{Ca} + \text{Mg}^* + \text{O}$ versus $\square + \text{Al}^* + \text{OH}^*$ diagram. As such, the trends of these data

deviate slightly from the hypothetical slopes of -0.5 and -1.0 , respectively. Within individual plots in Figures 6a, 6b, 7a and 7b, there may be several possible exchange-vectors that are consistent with the array of data. However, taken in sum, the exchange vector that most clearly accounts for the bulk of the substitutions involving Ca is $\text{CaMgO}_{-1}\text{Al}_{-1}(\text{OH})_{-1}$.

Although $\text{CaMgO}_{-1}\text{Al}_{-1}(\text{OH})_{-1}$ apparently accounts for most of the incorporation of Ca, the direction and the magnitude of the deviation of the data array from expected slopes are most consistent with the exchange vector $\text{CaMgNa}_{-1}\text{Al}_{-1}$ also being operative. This substitution apparently takes place, even though there is an adequate amount of Al to algebraically account for the entire Z site. The existence of the exchange vector $\text{CaMgNa}_{-1}\text{Al}_{-1}$ substitution is consistent with either the site substitution $^x\text{Ca} + ^z\text{Mg} = ^x\text{Na} + ^z\text{Al}$ or $^x\text{Ca} + ^y\text{Mg} = ^x\text{Na} + ^y\text{Al}$ (Table 3). However, optical (Mattson & Rossman 1987) and Mössbauer spectroscopic studies (Ferrow *et al.* 1988) of mixed-valence Fe-bearing aluminous tourmaline have suggested that a certain portion of the Fe^{2+} occupies the Z site, with Fe^{3+} in the Y site. This finding implies that substitution in the latter site is likely to develop such that a certain proportion of divalent cations (primarily Mg and Fe^{2+}) also are found at the Z site, with an additional amount of trivalent cations at the Y site.

Significant X-site vacancies in tourmaline are relatively common in many rock types. The compilation

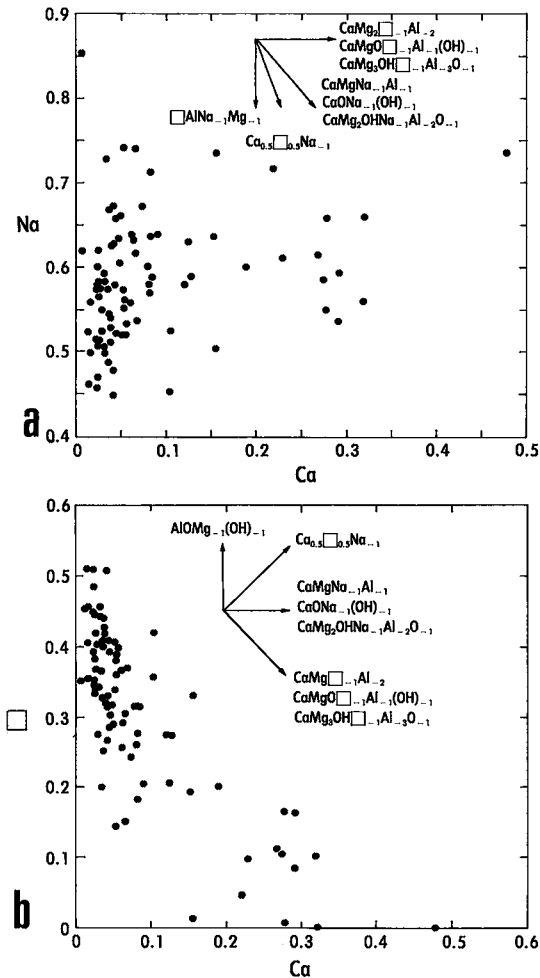


FIG. 6. Correlation of *X*-site constituents with Ca contents in 75 samples of natural tourmaline from a variety of bulk compositions (data of Povondra 1981). (a) Ca versus Na in atoms per formula unit. (b) Ca versus *X*-site vacancies.

by Werding & Schreyer (1984) of 213 natural tourmaline compositions from disparate rock-types clearly shows the importance of *X*-site vacancies in tourmaline. They found a range of *X*-site vacancies of 0–0.78 apfu, with an approximate mean of 0.3. Furthermore, they were able to synthesize the alkali-free tourmaline end-member, and to establish the importance of the exchange vector $\square\text{AlNa}_{-1}\text{Mg}_{-1}$. They pointed out that this substitution will be most strongly favored in those relatively unusual rocks whose compositions are both peraluminous and Na-Ca-deficient. Tourmaline from rocks such as the silicified komatiites and cherts found in South Africa illustrates this phenomenon in that it commonly

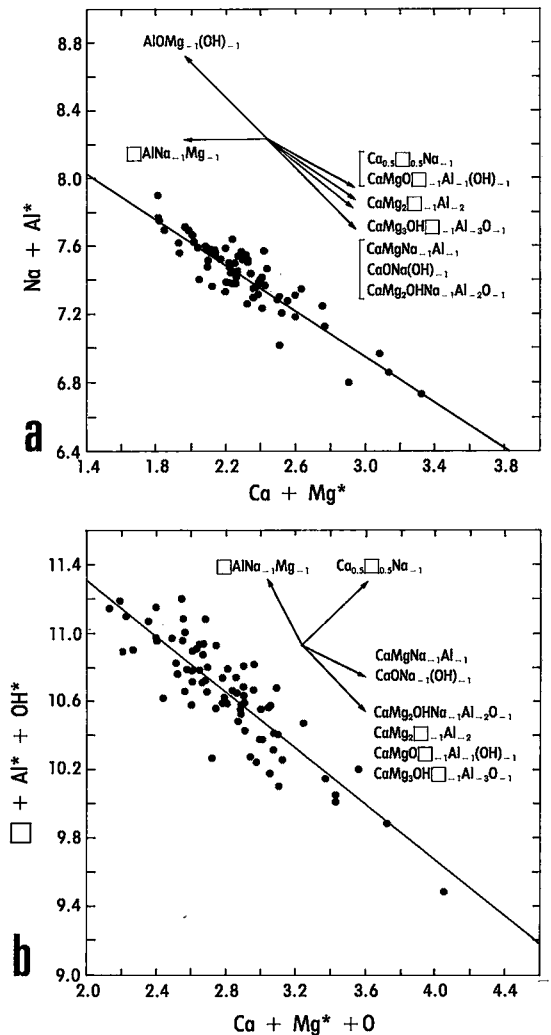


FIG. 7. Correlation of the product and reactant parameters projected to the Mg-Al subsystem for the complete dataset of tourmaline compositions of Povondra (1981). (a) Ca + Mg* versus Na + Al*. (b) Ca + Mg* + O versus $\square + \text{Al}^* + \text{OH}^*$. The * denotes multicomponent compositions projected to the subsystem used for plotting. The lines in both diagrams represent a linear least-squares fit to the data (see text for discussion of the projection parameters and the fit to the data).

contains 0.6–0.8 *X*-site vacancies (Byerly *et al.* 1986). However, in accordance with $\text{CaMgO}\square_{-1}\text{Al}_{-1}(\text{OH})_{-1}$, the addition of Ca to the tourmaline will tend to diminish the *X*-site vacancies. In fact, this exchange vector can be used, to a first approximation, to project tourmaline back to a Ca-free basis to establish the amount of hypothetical Ca-free tourmaline *X*-site vacancies.

SUMMARY AND CONCLUSIONS

This study evaluated possible Ca incorporation schemes in low-Li aluminous tourmaline. There are several useful findings:

(1) To isolate substitutions in tourmaline (or any solid-solution phase), the use of zoned tourmaline in conjunction with hypothetical composition-volumes defined by particular exchange-vectors are especially effective. The approach also allows minor substitutions to be identified.

(2) The exchange-vector diagrams (and their projections) are somewhat unorthodox but have several very useful features (Burt 1989). (a) The compositional data can be plotted directly on the diagrams without renormalization (as is necessary for most binary or ternary representations). (b) Several alternative plotting parameters can be used, so that there are other ways of locating the tourmaline data on the diagrams. This approach is especially important in those diagrams involving OH as a parameter, as the H contents in minerals cannot be determined on the electron microprobe. (c) Data from complex chemical systems can readily be reduced to the appropriate subsystem by "projection" down the exchange vectors.

(3) The incorporation of Ca into Li-poor aluminous tourmaline seems to be controlled by $\text{CaMgO}_{-1}\text{Al}_1(\text{OH})_{-1}$. This substitution was established using a chemically zoned Mg-rich tourmaline porphyroblast from a Mg-rich amphibolite from the Newry mines area, northwestern Maine. This sample proved to be ideal because it contains few other constituents that would obscure the mechanism of Ca incorporation. Using the exchange-vector diagrams, it was found that in addition to the dominant $\text{CaMgO}_{-1}\text{Al}_1(\text{OH})_{-1}$ substitution, there are also minor $\text{CaMgNa}_1\text{Mg}_{-1}$ and $\text{AlOMg}_{-1}(\text{OH})_{-1}$ substitutions that produce a slight dispersion of the tourmaline data.

(4) To further test the $\text{CaMgO}_{-1}\text{Al}_1(\text{OH})_{-1}$ substitution mechanism, a hypothetical Ca-Mg deprotonated composition, $\text{CaMg}_3\text{Al}_6(\text{BO}_3)_3\text{Si}_6\text{O}_{18}\text{O}(\text{OH})_3$, was synthesized at 820°C and 20 kbars.

(5) The validity of a given scheme of substitution [such as the $\text{CaMgO}_{-1}\text{Al}_1(\text{OH})_{-1}$ scheme] can be shown to hold for a number of different bulk-compositions if complete tourmaline compositions are available and the data are projected to the appropriate subsystem with the exchange vectors that define the composition of the tourmaline. Using this approach on tourmaline from a variety of bulk compositions, further confirmation established that $\text{CaMgO}_{-1}\text{Al}_1(\text{OH})_{-1}$ is the dominant mode of Ca-incorporation, but that a $\text{CaMgNa}_1\text{Al}_1$ substitution may also develop, even in tourmaline with sufficient amounts of trivalent cations to fill the Z site.

This latter result brings into question the common practice of initially assigning only trivalent cations to the Z site and then filling any deficit with divalent cations. Instead, this should be considered a limiting assumption.

(6) The combination of analysis of the characteristics of zoned minerals, coupled with attempted verification by synthesis experiments, is very powerful and should be used wherever possible to derive actual (as distinct from algebraically possible) mechanisms of substitution in minerals.

ACKNOWLEDGEMENTS

This work was supported by National Science Foundation, Grant EAR 8805220 to D.J. Henry and B.L. Dutrow. The text has greatly benefitted from discussions with C.V. Guidotti and thorough reviews by D.M. Burt, F.C. Hawthorne and E. S. Grew. We thank D.M. Burt for a preprint of his tourmaline vector-representation paper. B.L.D. acknowledges the support of the Alexander von Humboldt Foundation and W. Schreyer for the opportunity to use the experimental facilities of the Institut für Mineralogie at Ruhr-Universität. We also thank A. Fisher and K. Lyle for their expert photographic work, K. Oly for assistance with the SEM, and J. Jackson for typing the many tables in the text.

REFERENCES

- ABRECHT, J. & HEWITT, D.A. (1988): Experimental evidence on the substitution of Ti in biotite. *Am. Mineral.* **73**, 1275-1284.
- ALTY, S.W. (1933): Some properties of authigenic tourmaline from Lower Devonian sediments. *Am. Mineral.* **18**, 351-355.
- BASTIN, E.S. (1911): Geology of the pegmatites and associated rocks of Maine. *U.S. Geol. Surv. Bull.* **445**.
- BARTON, R., JR. (1969): Refinement of the crystal structure of buergerite and the absolute orientation of tourmalines. *Acta Crystallogr.* **B25**, 1524-1533.
- BENCE, A.E. & ALBEE, A.L. (1968): Empirical correction factors for the electron microanalysis of silicates and oxides. *J. Geol.* **76**, 382-403.
- BURT, D.M. (1988): Vector representation of phyllosilicate compositions. In *Hydrous Phyllosilicates Exclusive of Micas* (S.W. Bailey, ed.). *Rev. Mineral.* **19**, 561-600.
- (1989): Vector representation of tourmaline compositions. *Am. Mineral.* **74**, 826-839.
- BYERLY, G.R., CARPENTER, P., HENRY, D.J. & LOWE, D.R. (1986): Tourmalines of the Barberton greenstone belt. *Geol. Soc. Am. Abstr. Programs* **18**, 554.

- DIETRICH, R.V. (1985): *The Tourmaline Group*. Van Nostrand Reinhold, New York, N.Y.
- DONNAY, G. & BUERGER, M.J. (1950): The determination of the crystal structure of tourmaline. *Acta Crystallogr.* **3**, 379-388.
- FERROW, E.A., ANNERSTEN, H. & GUNAWARDANE, R.P. (1988): Mössbauer effect on the mixed valence state of iron in tourmaline. *Mineral. Mag.* **52**, 221-228.
- FOIT, F.F., JR. & ROSENBERG, P.E. (1977): Coupled substitutions in the tourmaline group. *Contrib. Mineral. Petrol.* **62**, 109-127.
- _____ & _____ (1979): The structure of vanadium-bearing tourmaline and its implications regarding tourmaline solid solutions. *Am. Mineral.* **64**, 788-798.
- FRASER, H.J. (1930): Paragenesis of the Newry pegmatite, Maine. *Am. Mineral.* **15**, 349-364.
- FUGE, R. & POWER, G.M. (1969): Chlorine in tourmaline from SW England. *Mineral. Mag.* **37**, 293-294.
- GONZALEZ-CARRENO, T., FERNANDEZ, M. & SANZ, J. (1988): Infrared and electron microprobe analysis of tourmalines. *Phys. Chem. Miner.* **15**, 452-460.
- GREW, E.S. & SANDIFORD, M. (1984): A staurolite-talc assemblage in tourmaline-phlogopite-chlorite schist from northern Victoria Land, Antarctica, and its petrogenetic significance. *Contrib. Mineral. Petrol.* **87**, 337-350.
- GUIDOTTI, C.V. (1970): Metamorphic petrology, mineralogy, and polymetamorphism in a portion of north-west Maine. *New England Intercoll. Geol. Conf. 62nd Ann. Meeting*, **B-2**, 1-23.
- HENRY, D.J. & GUIDOTTI, C.V. (1985): Tourmaline as a petrogenetic indicator mineral: an example from the staurolite-grade metapelites of NW Maine. *Am. Mineral.* **70**, 1-15.
- HEWITT, D.A. & ABRECHT, J. (1986): Limitation on the interpretation of biotite substitutions from chemical analyses of natural samples. *Am. Mineral.* **71**, 1126-1128.
- HOLDAWAY, M.J., DUTROW, B.L. & HINTON, R.W. (1988): Devonian and Carboniferous metamorphism in west-central Maine: the muscovite-almandine geobarometer and the staurolite problem revisited. *Am. Mineral.* **73**, 20-47.
- _____, GUIDOTTI, C.V., NOVAK, J.M. & HENRY, W.B. (1982): Polymetamorphism in medium- to high-grade pelitic metamorphic rocks, west-central Maine. *Geol. Soc. Am. Bull.* **93**, 572-584.
- MASSONNE, H.-J. & SCHREYER, W. (1986): High-pressure syntheses and X-ray properties of white micas in the system K_2O - MgO - Al_2O_3 - SiO_2 - H_2O . *Neues Jahrb. Mineral., Abh.* **153**, 177-215.
- MATTSON, S.M. & ROSSMAN, G.R. (1987): Fe^{2+} - Fe^{3+} interactions in tourmaline. *Phys. Chem. Miner.* **14**, 163-171.
- NĚMEC, D. (1969): Fluorine in tourmalines. *Contrib. Mineral. Petrol.* **20**, 235-243.
- PLYUSNINA, I.I. & VOSKRESENSKAYA, I.E. (1974): A more exact definition of certain positions in tourmaline through infrared spectroscopy. *Moscow Univ. Vest. Ser.* **29**, 38-42.
- POVONDRA, P. (1981): The crystal chemistry of tourmalines of the schorl-dravite series. *Acta Univ. Carol. - Geol.* **1981**, 223-264.
- ROSENBERG, P.E. & FOIT, F.F., JR. (1979): Synthesis and characterization of alkali-free tourmaline. *Am. Mineral.* **64**, 180-186.
- _____ & _____ (1985): Tourmaline solid solutions in the system MgO - Al_2O_3 - SiO_2 - B_2O_3 - H_2O . *Am. Mineral.* **70**, 1217-1223.
- _____, _____ & EKAMBARAM, V. (1986): Synthesis and characterization of tourmaline in the system Na_2O - Al_2O_3 - SiO_2 - B_2O_3 - H_2O . *Am. Mineral.* **71**, 971-976.
- THOMPSON, J.B., JR. (1982): Composition space: an algebraic and geometric approach. In *Characterization of Metamorphism through Mineral Equilibria* (J.M. Ferry, ed.). *Rev. Mineral.* **10**, 1-31.
- TSANG, T. & GHOSE, S. (1973): Nuclear magnetic resonance of 1H , 7Li , ^{11}B , ^{23}Na and ^{27}Al in tourmaline (elbaite). *Am. Mineral.* **58**, 224-229.
- WEINER, K.L. & GLAS, M. (1985): Was it turmalin? Symmetrie - bauplan - eigenschaften. *Mineral. München* **85**, 3-14.
- WERDING, G. & SCHREYER, W. (1984): Alkali-free tourmaline in the system MgO - Al_2O_3 - B_2O_3 - SiO_2 - H_2O . *Geochim. Cosmochim. Acta* **48**, 1331-1344.
- WILSON, G.C. & LONG, J.V.P. (1983): The distribution of lithium in some Cornish minerals: ion microprobe measurements. *Mineral. Mag.* **47**, 191-199.

Received March 23, 1989, revised manuscript accepted September 22, 1989.